Environmental Science and Pollution Research (2023) 30:22413–22429
https://doi.org/10.1007/s11356-022-23510-x

RESEARCH ARTICLE

Anti-angiogenic effects of aqueous extract from *Agrostemma githago* L. seed in human umbilical vein endothelial cells via regulating Notch/VEGF, MMP2/9, ANG2, and VEGFR2

Ali Niapour[1] · Mansour Miran[2] · Naisana Seyedasli[3,4] · Firouz Norouzi[5]

Received: 5 September 2021 / Accepted: 4 October 2022 / Published online: 26 October 2022

Abstract

Abnormal angiogenesis contributes to the pathogenesis of various diseases. The medicinal usage of *Agrostemma githago* L. seed (*A. githago* herein) has been stated in traditional medicine. This study aims to investigate the anti-angiogenic potential of aqueous extract of *A. githago*. In order to test the effect of *A. githago* extract, its impact on HUVECs, T98G, and HGF2PI2 cells was assessed by looking at cellular viability, changes in the distribution of cells in different phases of the cell cycle, induction of oxidative stress, and apoptosis. In addition, the release of VEGF, ANG2, and MMP2/9 factors, along with the expressions of the critical Notch signaling pathway players and VEGF receptors (VEGFR), was measured. Furthermore, a γ-secretase inhibitor (LY411575) was applied to determine whether Notch inhibition restores *A. githago* effects. As a further characterization, total phenolic and flavonoid contents of *A. githago* were estimated, and five triterpene saponin compounds were identified using LC–ESI–MS. In response to *A. githago* extract, a reduction in total cell viability, along with the induction of ROS and apoptosis, was detected. Exposure to the *A. githago* extract could modulate the release of VEGF and ANG2 from T98G and HUVECs, respectively. In addition, *A. githago* reduced the release of MMP2/9. Furthermore, Notch1, DLL4, and HEY2 transcripts and protein expressions were up-regulated, while VEGFR2 was down-regulated in treated HUVEC cells. Treatment with the *A. githago* extract resulted in a dose-dependent inhibition of AKT phosphorylation. Inhibition of Notch signaling retrieved the viability loss, reduced intracellular ROS, and alleviated the impaired tube formation in *A. githago*-treated HUVECs. Overall, these data underscore the anti-angiogenic potential of *A. githago* via inducing apoptosis, modifying the expression levels of VEGF/VEGFR2, and impacting the release of MMP2/9 and ANG2, effects that are most probably modulated through the Notch/VEGF signaling axis.

Keywords *Agrostemma githago* · HUVECs · Survival · VEGFR2 · Notch signaling · MMP2/9

Responsible Editor: Mohamed M. Abdel-Daim

✉ Ali Niapour
a.niapour@arums.ac.ir; ali.niapoor@gmail.com

[1] Research Laboratory for Embryology and Stem Cells, Department of Anatomical Sciences, School of Medicine, Ardabil University of Medical Sciences, Ardabil, Iran

[2] Department of Pharmacognosy, School of Pharmacy, Ardabil University of Medical Sciences, Ardabil, Iran

[3] School of Medical Sciences, Faculty of Medicine and Health, University of Sydney, Westmead Hospital, Westmead NSW, Sydney, Australia

[4] The Centre for Cancer Research, The Westmead Institute for Medical Research, Westmead NSW, Sydney, Australia

[5] Department of Genetics, School of Medicine, Ardabil University of Medical Sciences, Ardabil, Iran

Introduction

The formation of a new vessel from pre-existing endothelium is known as angiogenesis. This phenomenon plays a fundamental role in various physiological and pathological conditions such as wound healing, female reproduction cycle, inflammation, diabetes, and cancer progression (Kim and Byzova 2014). Angiogenesis commences with endothelial cell stimulation and continues with the degradation of the underlying basement membrane, endothelial cell proliferation and migration, and the establishment of new capillary structures (Lugano et al. 2020).

The Notch signaling, the vascular endothelial growth factor (VEGF)-receptor (VEGFR), and the tyrosine kinase with immunoglobulin-like and EGF-like domains (Tie) receptor–angiopoietin (ANG) pathways are essential factors in

regulating angiogenesis (Lugano et al. 2020). Notch signaling is a ligand-receptor signaling cascade that critically regulates angiogenesis and vessel hemostasis during embryonic development and adulthood. In mammals, five ligands, including delta-like (DLL1-4) and Jagged1-2, and four transmembrane receptors (NOTCH 1–4) have been identified for the Notch signaling pathway. The ligand-receptor binding triggers several proteolytic cleavages in the Notch receptor. A complex enzyme known as γ-secretase is responsible for releasing the Notch intracellular domain (NICD). Translocation of NICD into the nucleus activates the specific target genes, the HES and HEY family, and regulates endothelial cell fate decisions. It has been shown that NOTCH1, 3, and 4 and Jagged1-2 and DLL4 are involved in vascular formation and maintenance (Jakobsson et al. 2009; Maes et al. 2016; Tiemeijer et al. 2022).

VEGF-A is a potent stimulator of endothelial cells and inhibits their apoptosis. It has been shown that VEGFR2 mediates the primary angiogenic function of VEGF. Furthermore, the interaction between the Notch pathway and VEGF receptors (VEGFR) leads to the formation of vascular sprouts (Blanco and Gerhardt 2013, Garcia and Kandel 2012).

Angiopoietins are another family of growth factors with proven importance in angiogenesis. Angiopoietin-1 (ANG1) and angiopoietin-2 (ANG2) in conjunction with VEGF could modulate angiogenesis. It has been shown that ANG2 works with VEGF to facilitate cell proliferation and migration of endothelial cells. However, ANG2 promotes vessel regression without VEGF (Loutrari et al. 2004). Various therapeutic approaches have been developed to block the VEGF, the Notch receptors and ligands, and the receptor tyrosine kinase signaling. However, the high cost, acquired resistance, and induced toxicity in long-term exposure have limited the utilization of these agents as anti-angiogenic means, especially in cancer treatments (Caporarello et al. 2017; Liu et al. 2014).

The anti-inflammatory and anti-tumor properties of plant secondary metabolites have granted a considerable rationale for using medicinal plants to prevent or treat various diseases. Phytochemical compounds such as polyphenols, flavonoids, terpenoids, and saponins can modulate angiogenesis by regulating antioxidant activities and cellular signaling pathways (Adeola et al. 2021; Fan et al. 2006; Hassan et al. 2014; Lu et al. 2016). *Agrostemma githago L.* is a flowering plant of the *Caryophyllaceae* family, which is grown in many parts of the temperate world (Bohlooli et al. 2015). Diuretic, expectorant, and anthelmintic impacts of *Agrostemma githago* seeds have been stated in traditional medicine (Bohlooli et al. 2015). It has also been applied for solid tumor treatment in folk medicine (Foster et al. 1990). Avicenna, in his celebrated book "Canon of Medicine," has mentioned "Shooniz" as the local name of *A. githago* for treatment of wart and solid tumors (Avicenna 2014). We have demonstrated the anti-leishmaniosis activity of *A. githago* (Niapour et al. 2018). *A. githago* contains different types of triterpenoid saponins as well as agrostin 2, 5, and 6, which function as type 1 ribosome-inactivating proteins (RIPs) (Schrot et al. 2015). The anti-cancer effect of saponins has been widely demonstrated in the literature (Man et al. 2010; Vincken et al. 2007). It has been revealed that the combined application of saponins with anti-tumor drugs could intensify the toxicity of the chemotherapeutic agents (Melzig et al. 2005; Podolak et al. 2010). Furthermore, studies have shown that saponins, in conjunction with *A. githago*-derived agrostin, could modify cell membrane permeability and enhance the cytotoxic effect of the plant by a mechanism known as cooperative toxicity (Podolak et al. 2010). Bohlooli et al. have shown the apoptotic effect of *A. githago* on the AGS gastric cancer cell line (Bohlooli et al. 2015). It has been demonstrated that the *A. githago*-fractionated agrostin had an apoptotic effect on human leukemic cells by reducing Bcl-2 and induction of DNA damage (Chiu et al. 2001). The anti-angiogenic effect of saponins of natural extracts such as *Maesa lanceolate*, *Sea cucumber*, and *Momordica cymbalaria* has also been reported (Foubert et al. 2012; Tian et al. 2005). Therefore, this study aimed to investigate the anti-angiogenic properties of *A. githago* at the cellular and molecular levels.

Methods

Plant identification and extract preparation

A. githago seeds in complete ripeness (end of July) were collected from the suburban areas of Ardabil province, northwest Iran. After characterization by a botanist at the School of Agriculture, the University of Mohaghegh Ardabili, the *A. githago* plant was deposited in the herbarium of the School of Pharmacy, Ardabil University of Medical Sciences, by the No. ARD-1 voucher specimen (Bohlooli et al. 2015). *A. githago* seeds were used to prepare the aqueous extract. For this aim, seeds were dried and thoroughly ground. A definite amount of the resultant fine powder (100 g) was added to 500 ml of the distilled water. This mixture was stirred and homogenized for 15 min using an ultrasonic homogenizer (UP200H, Hielscher, Germany). After precipitating insoluble materials by centrifugation at 2600 rpm for 15 min, the supernatants were collected into new bottles and frozen at − 80 ℃. Bottles were freeze-dried (ALPHA 2-plus, Martin Christ, Germany) to obtain the lyophilized extract.

Estimation of total phenolic content

The Folin–Ciocalteu method was applied to determine the total phenolic content of the extract. Briefly, 100 µL of *A.*

githago extract (1 mg/ml) was mixed with 750 of Folin–Ciocalteu's phenol reagent for 5 min. Then, 750 µL of 20% (w/v) sodium carbonate solution was added. The total volume of the mixture was reached up to 3 mL with distilled water. The absorbance of the sample was measured at a wavelength of 750 nm using an ELISA Reader (Synergy HT, BioTek). Total phenolic content was calculated from the gallic acid standard graph equation and reported as mg of gallic acid per g dry weight of the extract.

Estimation of total flavonoids content

The aluminum chloride colorimetric method determined the total flavonoid content of *A. githago* extract. Briefly, 50 µL of *A. githago* extract (1 mg/ml) was mixed with 0.6 mL of 2% aluminum chloride. The solution was incubated for 60 min at room temperature, and the absorbance was read at 510 nm using an ELISA Reader. The total flavonoid content was calculated from the quercetin calibration plot and reported as mg quercetin per g dry weight of the extract.

Targeting extraction

The n-hexane solvent was used to remove lipids and other non-polar compounds. To end this, 10,000 ppm of the aqueous extract was dissolved in 60 ml of methanol. The later methanol extract was eluted by n-hexane. Finally, methanol extract free from non-polar compounds was obtained, and 20 µL of it was injected into the HPLC apparatus.

HPLC method

Liquid chromatography separations with a degasser, quaternary pump, and a PDA UV detector were performed on a Knauer Series 2000 system. Separation was carried out on RP-HPLC; 1 mg extract of the plant was dissolved in 1 mL methanol, and after centrifugation and filtering, 20 µL was injected in HPLC. The gradient program (Table 1) was carried out on C18-column (5 µm, 4.6 mm × 250 mm).

Mass spectrometry

Mass spectrometry was performed on a FinniganTM LCQTM DECA instrument equipped with an electrospray ionizer (ESI) and ion trap mass analyzer. The sample was analyzed in positive-ion mode at an *m/z* range of 100 – 200 Da. ESI–MS conditions were as follows: sheath gas flow rate: 80 mL min^{-1}; auxiliary gas flow rate: 20 mL min^{-1}; spray voltage: 5 kV; capillary temperature: 300 ℃; capillary voltage: 46 kV; tube lens – 60 kV; C and 5mC were identified at 112 m/z and 126 m/z, respectively. Xcalibur 2.0 SR2 software (copyright Thermo Electron Corporation 1998–2006) was used for data analysis.

Table 1 Gradient program of the HPLC

Time	Solvent A (H_2O)	Solvent B (MeOH)	Flow
0	95	5	1
30	30	70	1
45	0	100	1
55	0	100	1

Cell lines and culture

Human umbilical vein endothelial (HUVECs), glioblastoma (T98G), and fibroblastic (HGF2PI2) cell lines were purchased from the National Cell Bank of Iran (Pasteur Institute of Tehran, Iran). Cells were cultured in high glucose Dulbecco's Modified Eagle Medium (DMEM; Gibco: 12,800) containing 10% fetal bovine serum (FBS; Gibco: 10,270), 2 mM L-glutamine (Gibco: 25,030), 100 mg/ml streptomycin, 10,000 U/ml penicillin (Gibco: 15,140), and NEAA (Gibco: 11,140,050) at 37 ℃ in a humidified atmosphere of 5% CO_2. Cells in passages 5-15 were used in this study.

Cell viability assay

HUVECs, T98G, and HGF2PI2 at the density of 3×10^3 cells were plated onto each well of 96-well plates. Cells were treated with increasing concentrations (0-50 µg/ml) of aqueous extract of *A. githago* for 24 h, 48 h, and 72 h. Cell viability was assessed using an MTT assay (Niapour et al. 2015). Briefly, 0.5 mg/ml MTT solution (MTT; Sigma: M2128) was added to each culture well and incubated for four hours. The formazan crystals were then dissolved in dimethyl sulfoxide (DMSO; Sigma: D4540). The absorbance was measured at 570 nm by a microplate reader and reported as the percentage of cell viability relative to the control. The curve fitting was completed by nonlinear regression analysis in SigmaPlot software V12 (Systat Software, Inc., San Jose, CA, USA). The median inhibitory concentrations (IC50) were estimated using the four-parameter logistic model. In another set of experiments, HUVECs were treated with different concentrations of LY411575 (Cayman: 16,162) as a γ-secretase inhibitor (GSI) and 10 nM of LY411575 was accompanied by the IC50 dose of *A. githago*.

Growth curve

The cumulative cell counting in successive days of treatment was implemented to determine if the extract is slowing the growth of the cultures or actively reducing the number of cells compared with the start of the experiment. At each time point, the cell suspension was mixed with 0.4% trypan blue (Sigma: T6146) at a 1:1 ratio and counted using a hemocytometer. Trypan blue negative cells were counted on days 3, 5, and 7 from primary plating.

Cell cycle analysis

The flow-cytometry analysis was used to delineate the distribution of HUVECs in the different phases of the cell cycle. Briefly, HUVECs in control and *A. githago*-treated groups were stained with 4′,6-diamidino-2-phenylindole (DAPI; Sigma: D9542) and analyzed using Partec Space Flow Cytometer (Partec GmbH, Jettingen-Scheppach, Germany) (Mahmoudinia et al. 2019).

Apoptosis assay

Annexin V-FITC apoptosis detection (Abcam: ab14085) and Caspase-Glo 3/7 assay (Promega: G8090) kits were utilized to measure cell death mechanism(s) in *A. githago*-treated HUVECs. Apoptotic cells translocate phosphatidylserine (PS) from the inner leaflet of the cell membrane to the cell surface. Once on the cell surface, PS can be easily detected by staining with a fluorescent conjugate of annexin V. Propidium iodide (PI) binds tightly to the nucleic acids in the necrotic cells. Still, it is impermeant to alive or apoptotic cells. Briefly, cells in control and *A. githago*-treated groups were collected by centrifugation and resuspended in 1X binding buffer. Cells were stained with annexin V/PI at room temperature for 5 min and analyzed by a flow cytometer. Caspase 3/7 activity was measured as previously reported (Sharifi Pasandi et al. 2017). Briefly, equal volumes of cell suspension and kit reagent were mixed in white-walled 96-well plates, and the luminescence was detected after 3 h using a microplate reader at 570_{EM}. Treatment with cisplatin (15 µg/ml) was considered as a positive control in the caspase 3/7 assay.

Intracellular ROS assay

DCFDA cellular ROS detection assay kit (Abcam: ab113851) was applied to measure intracellular ROS (Mahmoudinia et al. 2019). Briefly, 24 h after plating 2.5×10^4 HUVECs onto each well of 96-well plates, they were stained with 25 µM DCFDA for 45 min at 37 ℃. Cells were then treated with *A. githago* (10 µg/ml) alone or *A. githago* + LY411575 (10 nM) for an hour. Tert-butyl hydrogen peroxide (TBHP) was used as a positive control. Based on kit protocol, 2′,7′-dichlorofluorescein diacetate (DCFDA) diffuses through cell membranes. Intracellular ROS oxidizes DCFDA into highly fluorescent 2′,7′-dichlorofluorescein (DCF). A fluorescence microplate reader can detect the latter compound at Ex $_{485}$/Em $_{535}$ nm. The fluorescence intensity is proportional to the ROS produced inside the cells. The ROS level in each group was reported as a percentage relative to the control.

Glutathione peroxidase activity assay

Glutathione peroxidase (GPx) activity was determined with a commercial kit (RANDOX Laboratories, Ltd.: RS504) as described before (Sharifi Pasandi et al. 2017). Briefly, cell lysates of *A. githago*-treated and untreated HUVECs were prepared, and GPx activity was measured. As the datasheet indicates, oxidized glutathione (GSSG) produced upon GPx activity in detoxifying hydroperoxide transforms into reduced glutathione (GSH) by glutathione reductase and NADPH consumption. The oxidation of NADPH to NADP + is accompanied by a decrease in absorbance at 340 nm.

Measurement of malondialdehyde level

Malondialdehyde (MDA) level was evaluated in the control group and *A. githago*-treated HUVECs, as described in the already published paper (Sharifi Pasandi et al. 2017). Briefly, 20% trichloroacetic acid (TCA; Merck: 76–03-9) was added to samples and standards and centrifuged at 3500 for 10 min. The supernatants were mixed with phosphoric acid (1%) (Merck: 109,286) and thiobarbituric acid (67%) (Merck: 504–17-6). After heating up for an hour at 95 ℃ and cooling down on the ice, n-butanol was used to precipitate the MDA-TBA adduct. MDA amount was measured using a spectrophotometer (UNICO: S-2100) at 532 nm. MDA amount was calculated through 1,1,3,3-tetra ethoxy propane (TEP) (Sigma: 122–31-6) standard graph equation.

Measurement of VEGF, ANG2, and MMP2/9 proteins

At each time point, the supernatants of T98G and HUVECs in control and *A. githago*-treated groups were collected and subjected to appropriate enzyme-linked immunosorbent assay (ELISA) kits to measure the protein levels of VEGF (R&D: DVE00), ANG2 (Abcam: ab99971), MMP2 (R&D: mmp200), and MMP9 (R&D: mmp900), respectively. According to the manufacturer's manual, the optical density was measured by a microplate reader at 450 nm. The absolute value of each protein was calculated according to the standard curve. Data was reported as a percentage of the control. All tests were implemented in duplicates (Saadati et al. 2021).

RNA extraction and real-time RT-PCR

Trizol reagent (Invitrogen: 15,596–026) was used to extract total RNA. Isolated RNA was treated with DNase I (Invitrogen: EN0521) to eliminate the contaminating genomic DNA. The RNA content in each sample was computed

utilizing Nanodrop (Thermo Fisher Scientific: ND-1000, USA). Complementary DNA (cDNA) was synthesized by the RevertAid™ First Strand cDNA Synthesis kit (Fermentas: K1622) according to the manufacturer's instructions. Real-time PCR was performed in a thermal cycler (Roche: 05,815,916,001) using SYBR Green Master Mix (EURx: E0402-01). The incubation condition includes denaturation for 10 min at 95 ℃ for one cycle, followed by amplification at 15 s at 95 ℃ and 45 s at 60 ℃ for 40 cycles. The relative expression level of each target gene versus the expression of the *GAPDH* as a housekeeping gene was calculated according to the $2^{-\Delta\Delta Ct}$ method (Niapour et al. 2019). The primer details are listed in Table 2.

Western blotting

After the completion of the treatments, cells were collected and washed twice with PBS. Cells were homogenized in a lysis buffer which contains 0.5% Nonidet P-40, 1% Triton X-100, 50 mM Tris–HCl (pH = 7.4), 150 mM NaCl, 1 mM DTT, 1 mM EDTA, 0.1% SDS, 1 mM EGTA, 2 mM PMSF, and 1% protease inhibitor cocktail. The lysates were centrifuged at 18,000 *g* for 10 min; the resulting supernatants were transferred to new tubes and stored at − 80 ℃. Protein concentrations were determined using the Bradford method. Equal amounts of proteins were separated by SDS-PAGE electrophoresis, and desired parts were transferred to PVDF membranes. The membranes were blocked for 1 h and then incubated for 2 h with primary antibodies (Table 3). After washing with TTBS, the membranes were probed with appropriate secondary antibodies (Table 2). Protein bands were visualized with the enhanced chemiluminescence (ECL) detection kit. β–actin was also detected as an internal control. The densitometric analysis of immunoreactive bands was performed by ImageJ software version 1.53 (NIH, Bethesda, USA) (Niapour and Seyedasli 2022).

Tube formation assay

The tube formation assay was used to evaluate endothelial cell angiogenesis in vitro (Niapour and Seyedasli 2022). To end this, 50 µL of ice-cold matrigel (Sigma: E1270) was added to each well and allowed to polymerize at 37 ℃ for 2 h. Then, HUVECs at 5×10^5/100 ml of DMEM supplemented with 5 ng/ml of bFGF (Sigma: F0291) were dispersed onto each well of the plate and incubated for 24 h in the presence of 10 µg/ml of *A. githago* alone or *A. githago* + LY411575 (10 nM). The enclosed network of tubes was photographed under an inverted microscope (Olympus: IX71) equipped with a digital camera (Olympus: D71), and the area of angiogenesis was measured using ImageJ software. All tests were applied in triplicates from three independent experiments.

Statistical analysis

The results were expressed as means ± SD. Data were analyzed using one-way ANOVA following post hoc Tukey's test to associate the means of all compared groups. Differences were considered significant at a level of $p < 0.05$.

Table 2 Primer sequences for real time-PCR

Gene	Primer Sequence (5'→3')	AT (℃)	Cycle	Accession No
NOTCH1	F: ACAGCGAGGAAGAGGAGGAC R: GGCATCAGAGCGTGAGTAGC	60	40	NM_017617.4
DLL4	F: CGCTACTGCTGCTGGTGG R: GACGACCGCCTGGAAGTG	60	40	NM_019074.3
HES1	F: GCTGGAGAAGGCGGACATT R: TGGACAGGAAGCGGGTCA	60	40	NM_005524.3
HES5	F: CGGTGGTGGAGAAGATGCG R: GCTTGGAGTTGGGCTGGTG	60	40	NM_001010926.3
HEY1	F: CGAGGTGGAGAAGGAGAGTG R: TGGGGACATGGAACCTAGAG	60	40	NM_012258.3
HEY2	F: TTGAGAAGACTTGTGCCAACTG R: GTGCGTCAAAGTAGCCTTTACC	60	40	NM_012259.2
VEGFR2 (KDR)	F: CCAAGAAGAACAGCACAT R: TTCCACCAGAGATTCCAT	60	40	NM_002253.3
VEGFR1(FLT1)	F: AATAAGCACACCACGCCCAG R: TCATCAGGGTAACTCCAGGTCA	60	40	NM_002019.4
NRARP	F: ACTGCGTGGTCAATGTGGTT R: AGAGGGAGAAGGAGGGAGGG	60	40	NM_006175.4
GAPDH	F: CCACTCCTCCACCTTTGACG R: CCACCACCCTGTTGCTGTAG	60	40	NM_002046.5

Table 3 Antibodies used in this study

Target phenotypes	Primary antibody	Host	Vender	Cat. number	Dilution
Notch receptor	Cleaved Notch1 (Val1744)	Rabbit	Cell signaling	4147 T	1:1000
Notch ligand	DLL4	Rabbit	Abcam	Ab176876	1:1000
Notch target gene	HEY2	Mouse	Abcam	ab167280	1 µg/ml
VEGF receptor	VEGFR2	Rabbit	Abcam	ab39256	1 µg/ml
VEGF receptor	VEGFR1	Mouse	Santa Cruz	sc-271789	1:1000
Akt pathway	AKT	Rabbit	Elabscience	E-AB-30471	1:1000
Akt pathway	p-Akt1/2/3 (B-5)	Mouse	Santa Cruz	sc-271966	1:1000
House keeping	β-Actin (C4)	Mouse	Santa Cruz	sc-47778	1:1000
Secondary Abs					
Conjugated with	Antibody	Vender	Cat. number	Isotype	Dilution
HRP	m-IgGκBP-HRP	Santa Cruz	sc-516102	IgG	1:5000
HRP	mouse anti-rabbit IgG-HRP	Santa Cruz	sc-2357	IgG	1:5000

Table 4 The total phenolic and flavonoid contents of *A. githago*

Sample	Phenolic content (mg GAE/100 g)	Flavonoid content (mg CUR/100 g)
Aqueous extract	17.75 ± 1.21	4.02 ± 0.12

Statistical analyses were performed with SPSS 15 for Windows.

Results

Analysis of phytochemical constituents of *A. githago* aqueous extract

The total phenolic and flavonoid content of *A. githago* was estimated (Table 4). After acquiring a suitable HPLC chromatogram, 20 µL of the methanol extract was injected into LC–MS. The chromatogram (Fig. 1A) and mass profiles were investigated in the positive mode. According to obtained mass profile from the LC–MS device and after comparing it with literature data (Clochard et al. 2020), five triterpene saponin compounds, including saponins A-D, were identified (Table 5 and Fig. 2A–D). The triterpene saponin E with m/z 1856 is agrostemmoside E which is probably found in *Agrostemma* species.

A. githago reduces cell survival and inhibits HUVECs proliferation

The cytotoxicity of *A. githago* was investigated via MTT assay and growth curve monitoring. Incubation with *A. githago* for 24 h decreased HUVECs viability up to 63.06 ± 2.48%, while treatment for 48 h and 72 h caused a significant decrease in cellular viability (Fig. 3A–E). The increment in *A. githago* concentration was accompanied by the lower viability of HUVECs and HGF2PI2 at 48 h or 72 h of treatment. These data indicate that *A. githago* reduces HUVECs and HGF2PI2 survival in a dose- and time-dependent manner. T98G cells were sensitive to the extract as compared with HUVECs and HGF2PI2. *A. githago* concentration above 1 µg/ml rocketed down the T98G viability in a way that the dose–response curve became linear at 10 µg/ml and higher concentrations on other cells. The IC50 was determined as 11.1 ± 0.5 µg/ml and 10 ± 0.5 µg/ml for HUVECs at 48 h and 72 h of *A. githago* treatment. The calculated IC50 was 3 ± 0.5 µg/ml and 4.6 ± 0.1 µg/ml for T98G and 12.2 ± 0.6 µg/ml and 10.9 ± 0.2 µg/ml for HGF2PI2 cells following 48 h and 72 h of treatment, respectively.

HUVECs growth kinetic was severely affected at 20–50 µg/ml of *A. githago*. However, on the 3rd day of the experiment, the cumulative number of HUVECs at 1–10 µg/ml of the extract was higher than the primary plating number at day zero. This limited growth of cells demonstrates the cytostatic effect of *A. githago* at lower concentrations. The reduced number of cells at 20–50 µg/ml of *A. githago* compared with the experiment's beginning indicates the cytocidal impact of the extract at higher concentrations. Although HUVECs recovered their growth by continuing the investigation, the number of HUVECs was prominently low at 30–50 µg/ml of *A. githago* (Fig. 4A).

A. githago halts cell cycle progression

The distribution of HUVECs in different cell cycle phases was assessed using flow-cytometry analysis. The percentages of the sub-G1 stage (apoptotic cells) were significantly increased after treatment with 10 (28.5 ± 2.5) µg/mL and 15 (47.5 ± 0.0) µg/mL of *A. githago* as compared with the control (8.1 ± 3.1). The population of cells in the G1 and G2/M phases was also reduced (Fig. 4B,C).

A. githago induces apoptosis

Annexin V-PI and caspase 3/7 assay were used to evaluate the induction of apoptosis after *A. githago* administration. Annexin

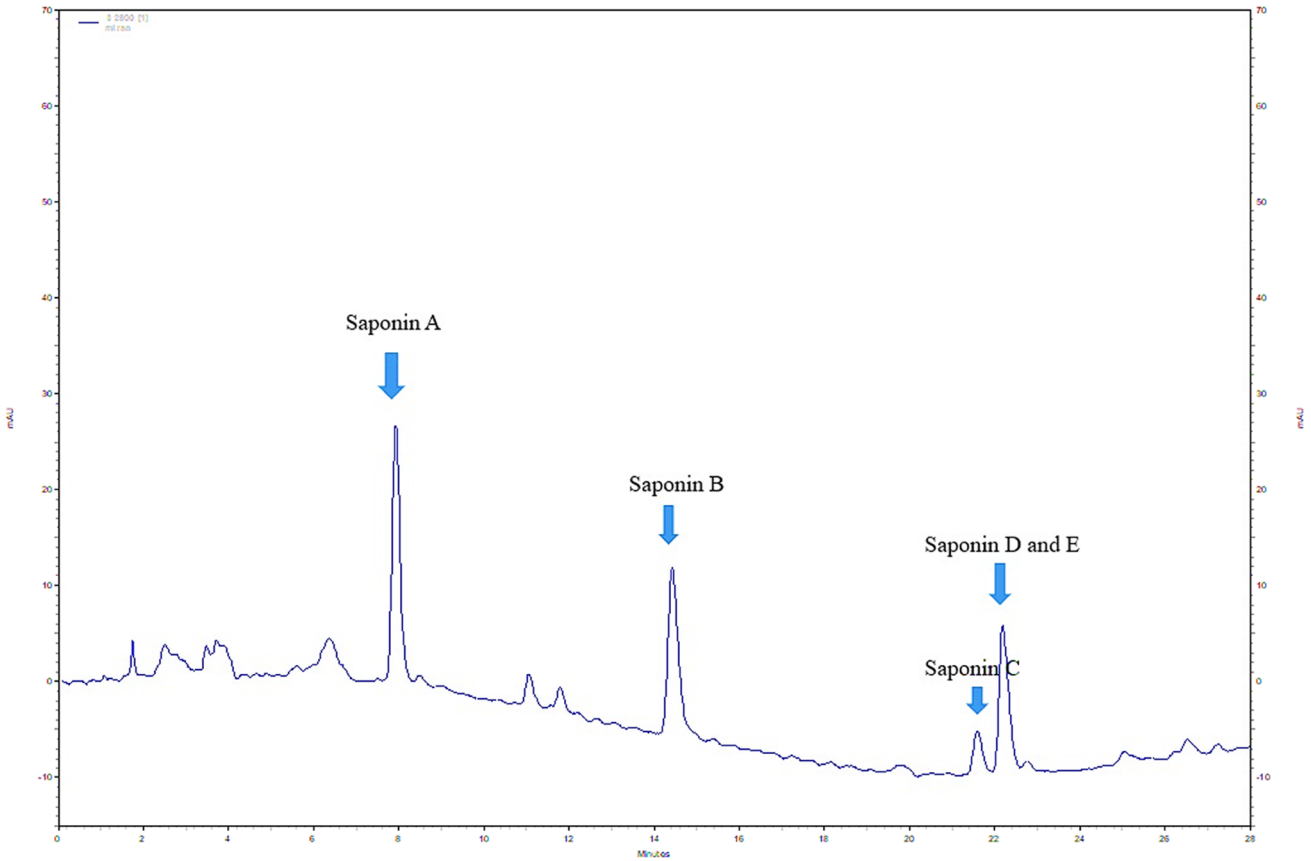

Fig. 1 HPLC chromatogram of *A. githago*. The chromatographic profile of *A. githago* methanol extract was illustrated

Table 5 Positive ion and Calcd. mass of identified triterpene saponin compounds from *A. githago* by LC–MS

Saponins	Positive ion	Calcd. mass
A	$C_{39}H_{62}O_{12}Na^+$	745.13
B	$C_{39}H_{62}O_{12}H^+$	869.67
C	$C_{45}H_{72}O_{17}Na^+$	907.81
D	H+H	1814/2 = 907
E	H+H	1856/2 = 928

V-PI flow-cytometry analysis showed a significant increase of early and late apoptotic cells in extract-received groups. Escalating *A. githago* concentration from 10 to 15 µg/ml resulted in a higher cell at the late apoptosis quadrant (Fig. 5A,B). In addition, the caspase 3/7 activity was increased in the *A. githago*-treated cells as compared with the control (Fig. 5C).

A. githago induces the generation of ROS in HUVECs

Production of oxidative stress was evaluated directly through the measurement of intracellular ROS and indirectly via the measurement of GPx activity and MDA level. Our results showed that the intracellular ROS was increased in *A. githago*-treated cells as compared with the control (Fig. 8C). The GPx activity was significantly decreased (Fig. 5D). At the same time, MDA content was augmented (Fig. 5E).

A. githago modifies VEGF and ANG2 release

The effect of *A. githago* on VEGF and ANG2 release from T98G and HUVEC cell lines was examined, respectively. Following incubation with 2 µg/ml and 3 µg/ml of *A. githago* extract, the VEGF release from T98G cells was reduced in a dose- and time-dependent manner (Fig. 6A). Treatment with 7 µg/ml and 10 µg/ml of *A. githago* extract for 24 h, 48 h, and 72 h increased the ANG2 protein levels in the supernatant of HUVECs. Moreover, ANG2 release was significantly higher in cells treated with 10 µg/ml of *A. githago* extract compared to 7 µg/ml (Fig. 6B).

A. githago decreases MMP2 and MMP9 levels

The MMP2 and MMP9 levels in the supernatant of the HUVECs and T98G cells were measured. The amount of

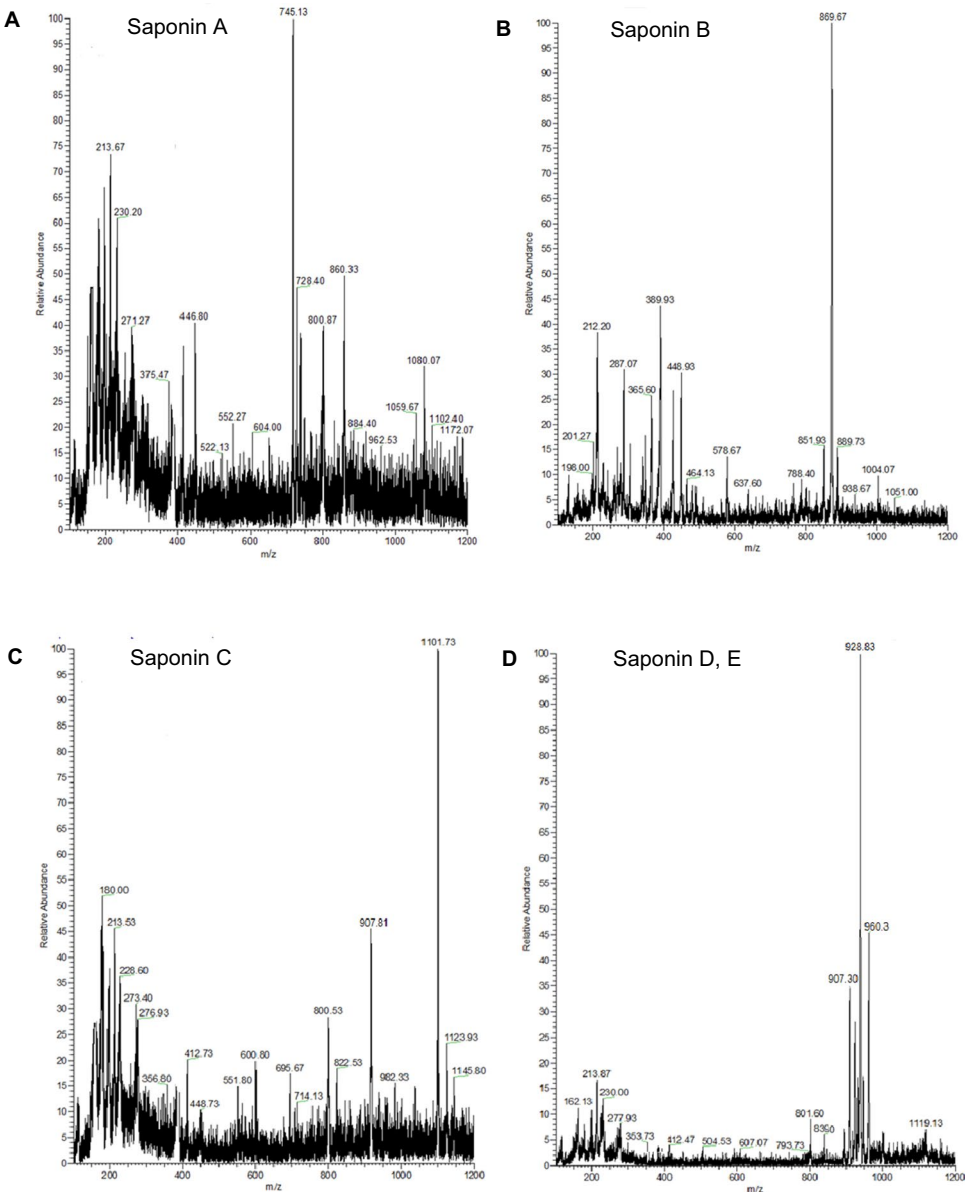

Fig. 2 Mass profile of saponins. The mass profile of five detected triterpene saponins from *A. githago* has been shown in parts **A** to **D**, respectively

these enzymes was noticeably higher in the collected supernatant of T98G cells than in HUVECs. Our results showed that the release of MMP2 and MMP9 was significantly decreased in both cell lines following *A. githago* extract treatment (Fig. 6C,D).

A. githago extract affects the players of the Notch signaling and VEGFR signaling pathways

The expression of crucial factors involved in Notch and VEGFR signaling which are known to inhibit angiogenesis were evaluated at transcript and protein levels. *NOTCH1*, *DLL4*, *HEY2*, *HES5*, and *VEGFR1* genes were up-regulated. In contrast, the *VEGFR2* gene expression was down-regulated (Fig. 7A). Western blot analysis confirmed that the protein levels of cleaved-NOTCH1, DLL4, and HEY2 were increased in a dose-dependent manner in cells treated with the *A. githago* extract (Fig. 7B,C). In the meantime, the VEGFR2 and p-AKT protein levels were reduced. HES1, HEY1, and NRARP expressions showed no statistically significant changes (Fig. 7A).

Pharmacological inhibition of Notch signaling attenuates the effects of *A. githago* on cell viability, ROS induction, and tube formation

LY411575 was used to inhibit the Notch pathway pharmacologically. First, we showed that LY411575 did not affect HUVECs viability (Fig. 8A). LY411575 at 10 nM and

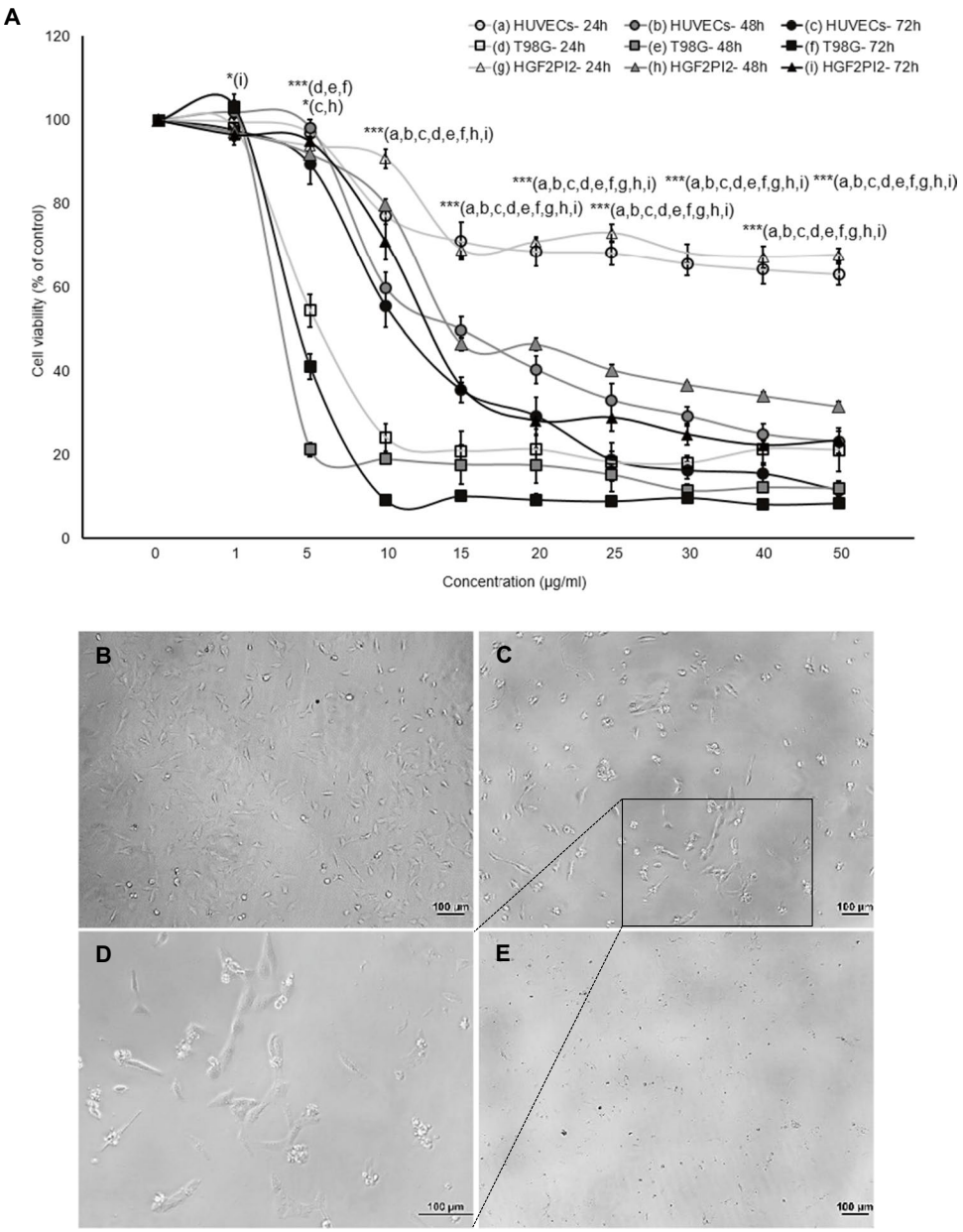

Fig. 3 Viability measurement. HUVECs, T98G, and HGF2PI2 cell lines were treated with *A. githago*, and their dose–response curves were plotted after 24 h, 48 h, and 72 h of treatment (**A**). Photomicrographs of HUVECs in control, 15 µg/ml and 30 µg/ml of *A. githago*-treaded groups were shown in **B**–**E**, respectively. Higher magnification of the boxed area in part **C** demonstrated some characteristics of apoptosis such as cell shrinkage and blebbing (**D**). $*p < 0.05$ and $***p < 0.001$ vs. control group

100 nM (data not shown) were applied to determine whether Notch inhibition reverses the toxic effects of *A. githago*. Our MTT assay showed that LY411575 could partially alleviate *A. githago* toxicity (Fig. 8B). LY411575 relatively reduced the intracellular ROS levels and relieved the impeded-capillary tube-like formation (Fig. 8C-H).

Discussion

Angiogenesis is a vital process in numerous physiological events, and its abnormality has been a treatment target in many angiogenic-dependent diseases. Medicinal plants and phytochemical compounds have long been investigated for inhibition or stimulation of angiogenesis (Lu et al. 2016). Our results showed that *A. githago* could decline the viability of HUVECs, T98G, and HGF2PI2 cells in a dose- and time-dependent manner. In line with our findings, other investigations have elucidated the cytotoxic effects of herbal extracts such as *Laggera alata* (Liang et al. 2017), *Artemisia sieberi* (Abdolmalekia et al. 2016), *Eugenia jambolana*, *Musa paradisiaca*, and *Coccinia indica* (M et al. 2017). Interestingly, the cytotoxic effect of *A. githago* was more potent on T98Gs than that of HUVECs. Next, we investigated the impact of *A. githago* on the viability of a fibroblastic HGF2PI2 cell line. Fibroblasts, considered a surrogate for the tissue-resident cells, are useful in vitro

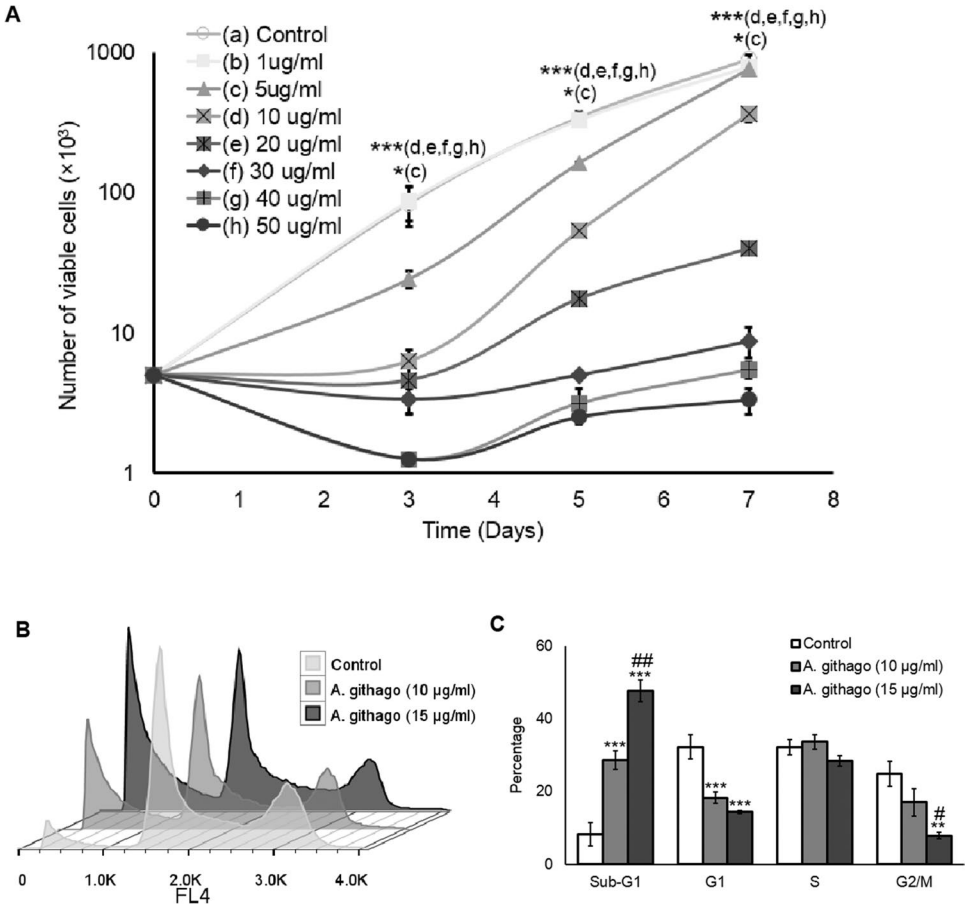

Fig. 4 Cumulative cell counting and cell cycle analysis. HUVECs were treated with increasing concentrations of *A. githago* for 48 h. The number of viable cells in successive days of counting was illustrated in part **A** using a semilog graph of cell number vs. days. The distribution of HUVECs in different phases of the cell cycle in the control and *A. githago* treatment groups were illustrated and quantified in **B** and **C**, respectively. $*p<0.05$, $**p<0.01$, and $***p<0.001$ vs. control group

model systems to surmise medication cytotoxicity and potential side effects (Jantova et al. 2016). The estimated IC50 for HGF2PI2 was 12.2 ± 0.6 and 10.9 ± 0.2 after 48 h and 72 h of *A. githago* administration, respectively. Although further investigations would be necessary, this finding suggests that *A. githago* may target cancerous cells at lower concentrations without affecting normal tissues. The cumulative cell counting revealed that HUVECs could recover their growth up to 20 µg/ml of *A. githago*. However, HUVECs proliferation was permanently impaired at higher concentrations. MTT assay and growth curve results suggest the antiproliferative effect of *A. githago* at lower concentrations and the cytocidal impact of the extract at higher concentrations. To further understand the underlying mechanism(s) of cell death, the induction of ROS and apoptosis were evaluated. The higher levels of intracellular ROS and MDA were accompanied by a significant reduction of GPx activity in *A. githago*-treated HUVECs. Annexin V/PI assay showed marked induction of early and late apoptosis following *A. githago* treatment. The increased sub-G1 peak and elevated caspase 3/7 activity confirmed the induction of apoptosis following *A. githago* treatment. Consistent with these data, it has been shown that treatment of HUVECs and MCF-7 cell lines with different concentrations of ethyl acetate extracts of *Eugenia jambolana* and *Musa paradisiaca* resulted in the cell cycle arrest and increased the sub-G1 population (Mohammadi-Motlagh et al. 2017). The elevated level of caspase-3 and reduced amount of Bcl-2 protein have been documented in AGS cells treated with *A. githago* (Bohlooli et al. 2015).

Tube formation assay is one of the rapid, well-established, and quantitative in vitro angiogenesis methods, exploiting the endothelial cell's ability to form three-dimensional capillary-like tubular structures (Niapour and Seyedasli 2022). Our results demonstrated that *A. githago* suppresses HUVECs tube formation. Numerous plant extracts, including *Vigna angularis* (Koon et al. 2018), *Brittle star* (Baharara et al. 2015), *Eugenia jambolana*, and *Musa paradisiaca* (Mohammadi-Motlagh et al. 2017), and plant-derived bioactive components such as 2-Methylpyridine-1-ium-1-sulfonate (MPS) from *Allium hirtifolium* (Mohammadi-Motlagh et al. 2017), Oridonin isolated *Rabdosia nervosa* (Dong et al. 2014), 5α-hydroxycostic acid and hydroxyisocostic acid isolated from the *Laggera alata* (Liang et al. 2017), Ziyuglycoside II of *Sanguisorba officinalis* (Nam et al. 2017), Tanshinone IIA from *Salvia miltiorrhiza* (Xing et al. 2015), Capsaicin from red pepper (Min et al. 2004), and Perillyl alcohol from mints and cherries (Loutrari et al. 2004), were used to inhibit HUVECs tube formation.

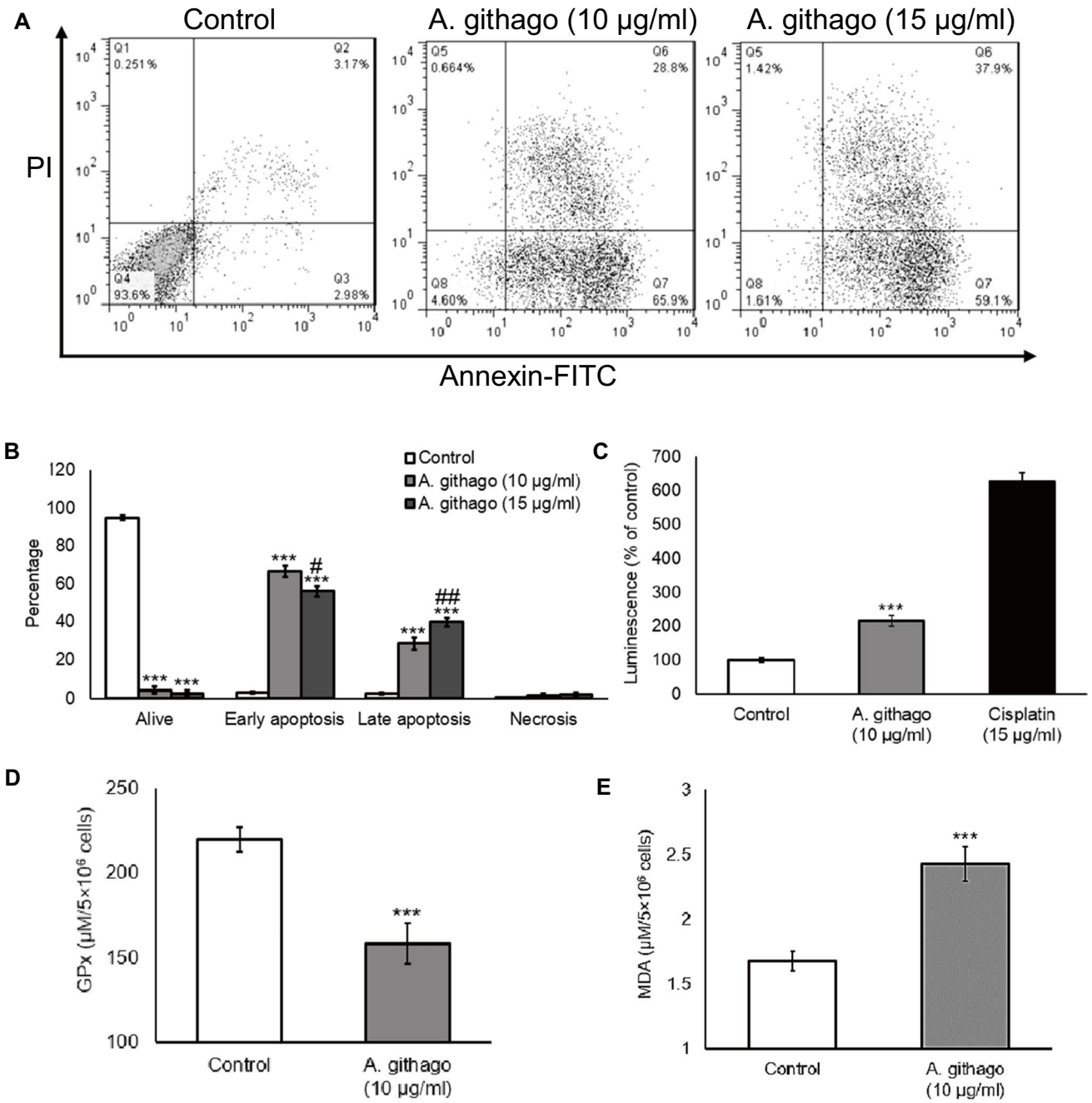

Fig. 5 Apoptosis and oxidative stress induction. HUVECs were treated with 10 µg/ml and 15 µg/ml of *A. githago* and then stained with a commercial annexin V/PI kit. The percentages of cells in four quadrants were illustrated in **A** and **B**. The caspase 3/7 activity, GPx, and MDA levels were shown in parts **C**, **D**, and **E**, respectively. ***$p < 0.001$ vs. control group. #$p < 0.05$ and ###$p < 0.001$ vs. *A. githago* (10 ug/ml)

Angiogenesis is controlled by a delicate balance between positive and negative regulators. VEGF is the classical angiogenic factor secreted in response to wounding, ischemia, or hypoxia by several cell types, including cancerous cells. VEGF activates endothelial cells mainly through VEGFR1 and VEGFR2. It has been shown that VEGFR2 mediates the primary angiogenic function of VEGF (Deryugina and Quigley 2015). It has been demonstrated that VEGF interaction with VEGFR1 could induce MMP9 induction and promote lung cancer metastasis (Hiratsuka et al. 2002). Glioblastoma is known for the high density of vessels in the tumor mass. Therefore, the inhibition of VEGF release from T98G cells was evaluated in this study. Our data indicated that *A. githago* could repress the VEGF release from

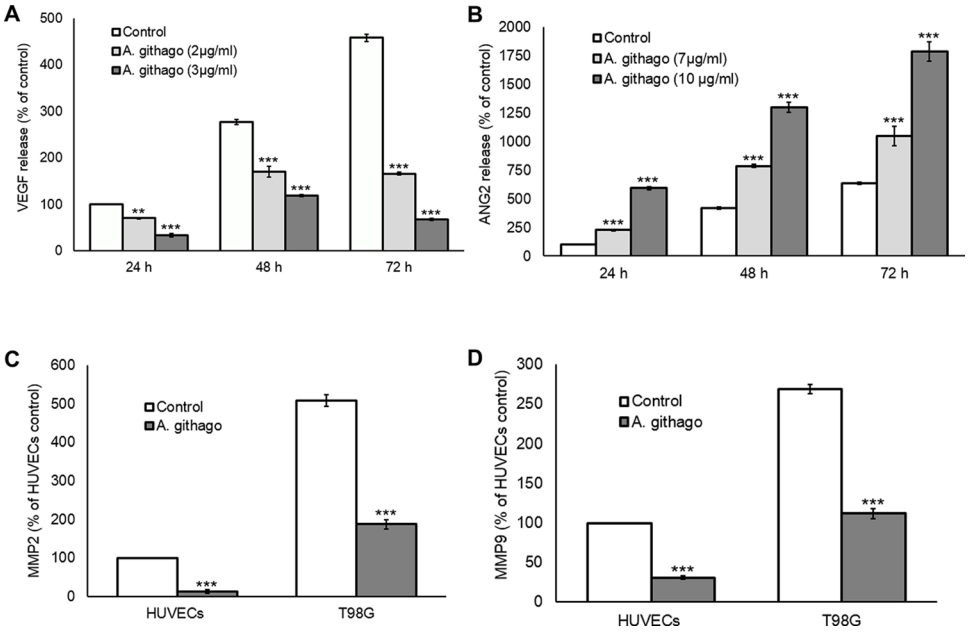

Fig. 6 VEGF, ANG2, and MMP2/9 release. HUVECs and T98G cells were treated with *A. githago*. VEGF release from T98G cells was illustrated in part **A**. The ANG2 secretion by HUVECs and MMP2/9 levels in the supernatant of HUVECs and T98G cells were represented in **B**–**D**, respectively. ***$p < 0.001$ vs. control group

T98G cells in a dose- and time-dependent manner. Loutrari et al. have shown the concentration and time-dependent decrease in the basal production of VEGF from K562 human lymphoblastoma cells, B16 mouse skin melanoma, and MDA-MB-231 human mammary gland cancer cell lines following perillyl alcohol treatment (Loutrari et al. 2004). Furthermore, the decrease in VEGF release from MHCC97H cells and HUVECs was attributed to the anti-angiogenic properties of *Scutellria barbata* extract (Dai et al. 2013). It has been shown that Ziyuglycoside II could reduce the phosphorylation of VEGFR-2, Src, Akt, JNK, ERK, and p38 mitogen-activated protein kinase (MAPK) in HUVECs (Nam et al. 2017).

Angiopoietins are another family of growth factors with proven importance in angiogenesis. Angiopoietin-1 (ANG1) and angiopoietin-2 (ANG2) in conjunction with VEGF could modulate angiogenesis. ANG2 is produced by endothelial cells and functions against ANG1-induced phosphorylation of TEK tyrosine kinase (Tie2) on vascular endothelium (Loutrari et al. 2004, Thurston and Daly 2012). It has been shown that ANG2 works with VEGF to facilitate cell proliferation and migration of endothelial cells (Akwii et al. 2019). However, ANG2 promotes vessel regression in the absence of VEGF (Loutrari et al. 2004, Thurston and Daly 2012). Our results demonstrated that *A. githago* increased ANG2 release in a dose- and time-dependent manner from HUVECs. In the same way, perillyl alcohol and its ester form reduced VEGF release from cancerous cells and attenuated the ANG2 secretion from endothelial cells in a concentration- and time-dependent manner (Loutrari et al. 2004). Furthermore, the treatment of *Laggera alata* (eudesmane-type sesquiterpenes) significantly down-regulated the VEGF-induced ANG2 expression in endothelial cells (Liang et al. 2017).

The matrix metalloproteinase-2 and -9 (MMP2/9) are involved in the degradation of extracellular matrices, providing endothelial sprouting and proliferation in provisional ECM (Senger and Davis 2011). MMP inhibitors putatively offer a preventive measure against angiogenesis and tumor metastasis. We found that *A. githago* decreased the protein level of MMP2 and MMP9 in the supernates of treated HUVECs. In line with these findings, it has been shown that *Davallia bilabiata* treatment reduced MMP2 secretion and augmented the tissue inhibitor of metalloproteinase-2 (TIMP-2) and reversion-inducing cysteine-rich protein with kazal motifs (RECK) levels (Liu et al. 2017). We also evaluated the MMP2/9 level in the T98G cell line supernatants. Glioblastoma is known for highly invasive growth, high expression of MMP2/9, and extensive neovascularization (Velasquez et al. 2019). Our results demonstrated that *A. githago* could significantly reduce the MMP2/9 levels in *A. githago*-treated T98G cells as compared with the control group. Cancer cells regulate MMP production in endothelial cells through VEGF (Deryugina and Quigley 2015) and Notch signaling (Funahashi et al. 2011). A study has shown that VEGF/VEGFR2 interaction down-regulates MMP9 expression via STAT1 activation and reduces B chronic lymphocytic leukemia (Ugarte-Berzal et al. 2010). On the other hand, MMP9 degrades the cellular matrix and releases bioactive VEGF (Lu et al. 2016).

The Notch signaling pathway is critical for proper vascular development. The equilibrium between DLL4-NOTCH1 as an inhibitory signal and Jagged-NOTCH1 as a pro-angiogenic cascade determines the possibility of vessel repression

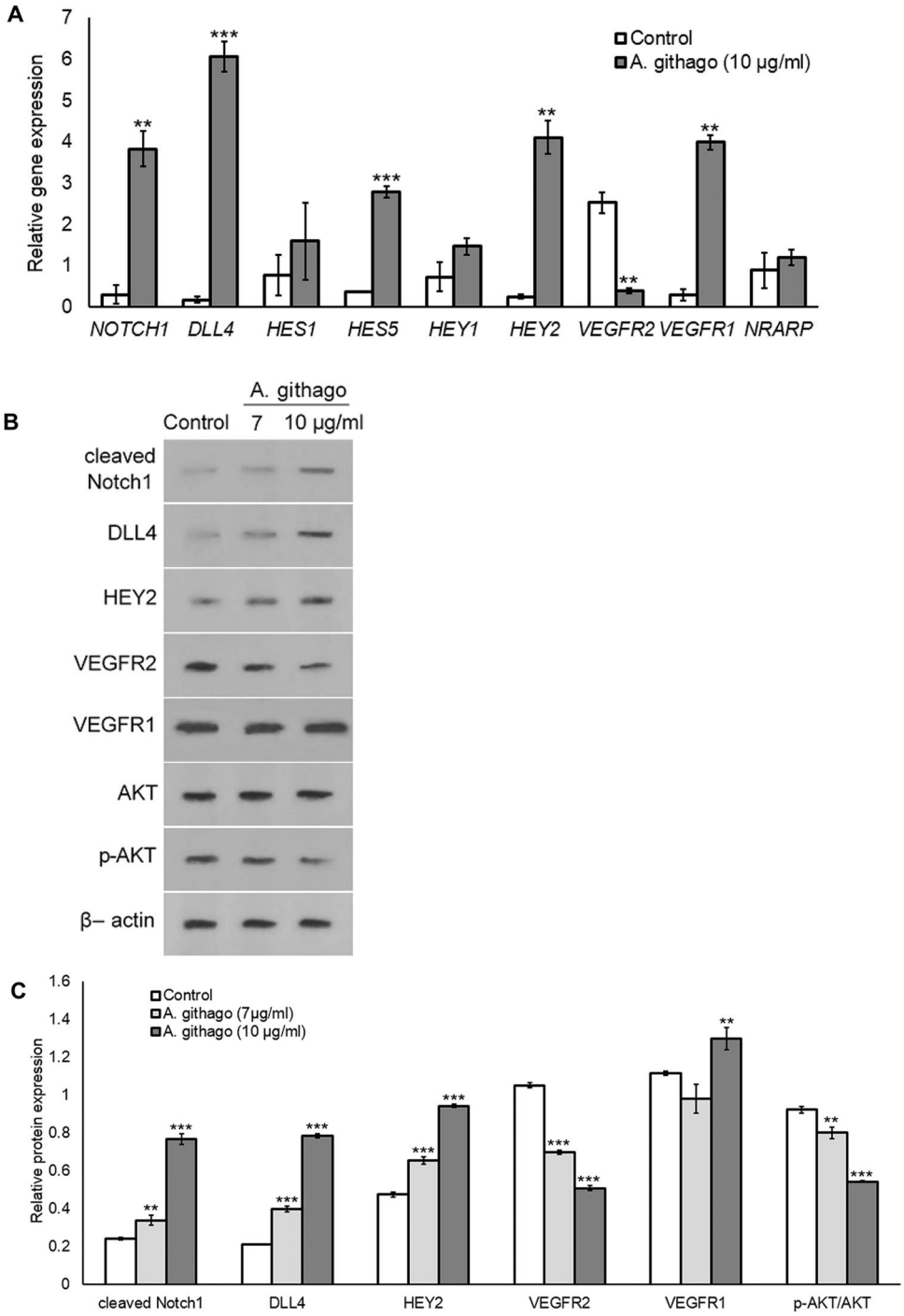

Fig. 7 Effect of *A. githago* on Notch signaling pathway, VEGFRs, and AKT/p-AKT ratio. The expression of some key Notch signaling and VEGFRs-related genes were assessed by real-time PCR (**A**). The results of western blotting were shown in part **B**. The relative densitometric analysis of immunoreactive bands was presented in part **C**. $^{**}p < 0.01$, $^{***}p < 0.001$ vs. control group

or sprouting (Antfolk et al. 2017; Chen et al. 2019). Compelling evidence indicates that the binding of VEGF to VEGFR2 up-regulates VEGFR2 and DLL4 expression in endothelial cells. This event determines the endothelial tip cell phenotype. DLL4 activates Notch signaling in adjacent cells through NOTCH1 interaction. The NOTCH1-activated cells become stalk cells and express more Notch targets like HES and HEY family and VEGFR1 (Chen et al. 2019, Phng and Gerhardt 2009). VEGFR1 and its soluble form act as a decoy in endothelial cells and regulate spatial activation of VEGFR2 and vessel sprouting (Thomas et al. 2013). Our results showed a significant decrease in VEGFR2 expression and a sharp increase in DLL4 and NOTCH1 profile expressions in *A. githago*-treated HUVECs. The level of HEY2 and HES5 was also increased. Translocation of NICD into the nucleus predominantly activates *HES* genes in the nervous, hematopoietic, endocrine, and immune systems, while *HEY* genes are critical for Notch

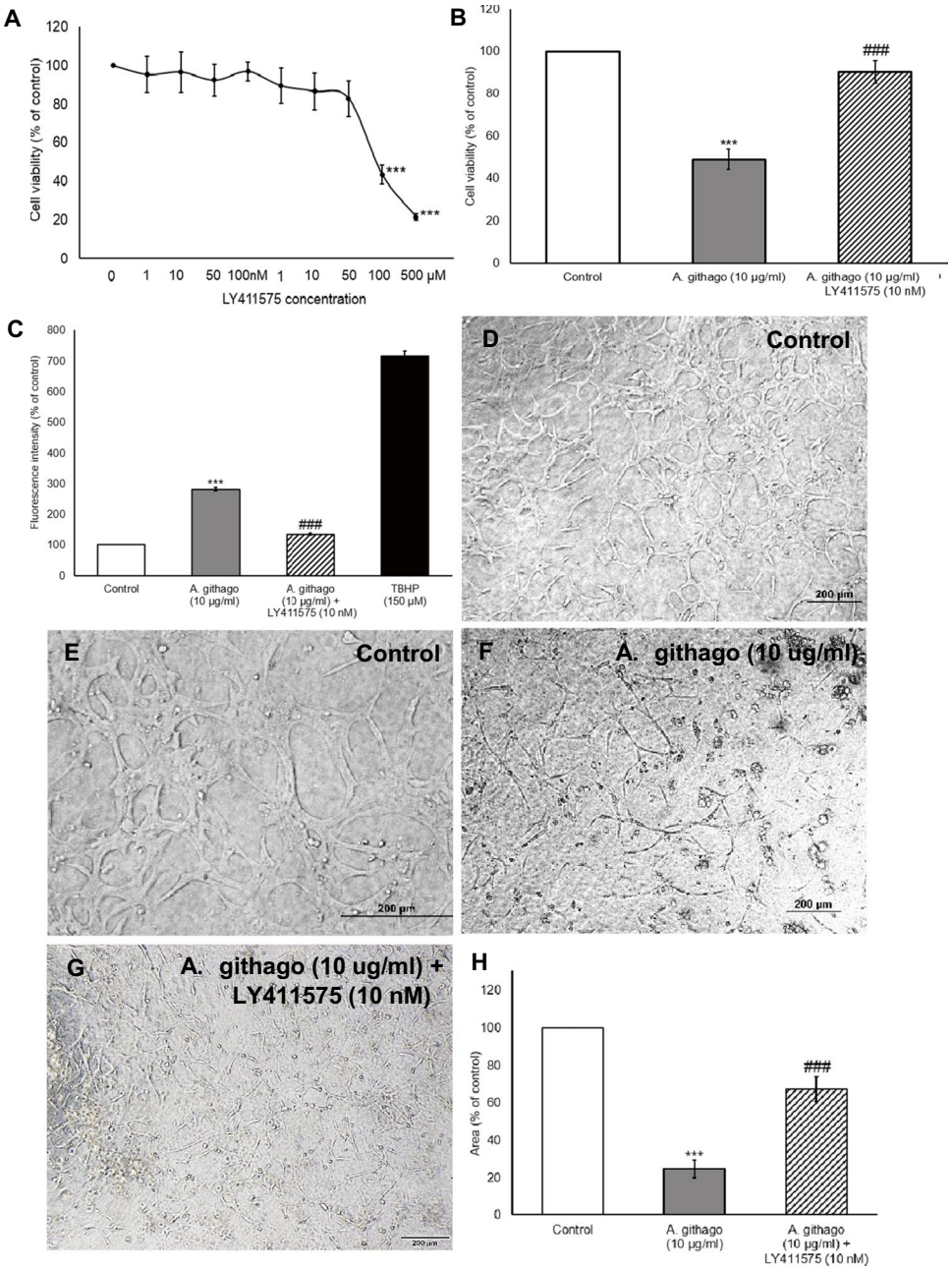

Fig. 8 Notch signaling inhibition and *A. githago* treatment. The possible effect of LY411575 as a GSI on HUVECs viability was assessed by MTT (**A**). *A. githago*-induced toxicity (**B**) and ROS (**C**) were relieved with GSI co-treatment. TBHP was used as a positive control in ROS assay HUVECs were able to form capillary-like structures on ECM (**D**). The higher magnification of the control group was shown in part **E**. *A. githago* treatment impaired tube formation capacity (**F**), while GSI administration ameliorated the tube formation capacity of HUVECs (**G**). The formation of tube-like structures in untreated HUVECs, *A. githago*, and *A. githago* + LY411575 received groups were quantified in part H. ***$p < 0.001$ vs. control group. ###$p < 0.001$ vs. *A. githago* (10 ug/ml)

signals in the cardiovascular system (Woltje et al. 2015). Notch indirectly inhibits VEGFR2 expression via HEY2 induction, whereas Notch activation induces VEGFR1 at the mRNA and protein levels (Kofler et al. 2011). Our findings were in line with these studies demonstrating essential transcript and protein changes favoring angiogenesis inhibition. Xing and colleagues have shown that the anti-angiogenic effect of Tanshinone IIA was mediated by the down-regulation of VEGFR2 and CD146 transcript and protein levels in HUVECs (Xing et al. 2015). Blocking of VEGF/VEGFR2 was the underlying anti-angiogenic mechanism of *Sanguisorba Officinalis*-derived Ziyuglycoside II (Nam et al. 2017). *Davallia bilabiata* inhibited the *VEGF-A*, *-B*, *-C*, *-D* and *VEGFR-1*, *-2*, *-3* gene expressions (Liu et al. 2017).

Finally, we wondered if Notch inhibition restores *A. githago* effects. Our result showed that pharmacological blockade of Notch signaling could partially recover HUVECs viability, reduce intracellular ROS, and alleviate *A. githago*-impaired tube-like formation. In line with these findings, Yang and colleagues have shown that implementation of N-[N-(3,5-difluorophenacetyl)-L-alanyl]-S-phenylglycine t-butyl ester (DAPT) or Notch1 siRNA could

significantly improve cellular viability, reduce oxidative stress, and down-regulate the NOTCH1 and HES1 expression in H2O2-treated HUVECs (Yang et al. 2013). Another study has demonstrated that endosulfan-induced cell viability loss, cell cycle arrest, and apoptosis were attenuated by pharmacological inhibition of Notch signaling. Moreover, the elevated expression of DLL4, NOTCH1, cleaved-NOTCH1, HES1, and P21 was reduced by DAPT administration (Wei et al. 2017).

Conclusion

A. githago reduced HUVECs viability and proliferation and induced apoptosis in the endothelial cell line. *A. githago* could inhibit angiogenesis via modifying VEGF, MMP2/9, and ANG2 liberations from the cancerous and endothelial cell lines. Although the DLL4-NOTCH1-VEGFR2 axis was shown to be modulated, further studies remain to fulfill these findings.

Acknowledgements We thank Dr. Bohlooli for providing the *A. githago githago* seed extract.

Author contribution Estimation of total phenol and flavonoid of the extract and LC–MS performance and interpretation were done by M.M. HUVECs, T98G, and HGF2PI2 culture, MTT assay, cell cycle analysis, annexin V-PI, caspase 3/7 assay, ROS, and ELISA kits were done by A.N. Primer design and real-time PCR were performed and interpreted by F.N and A.N. Study design: A.N. and N.S did statistical analyses and manuscript preparation. All authors read and approved the final manuscript.

Funding This study was financially supported by Ardabil University of Medical Sciences (Grant No. arums-199).

Data availability The datasets used and/or analyzed during the current study are available from the corresponding author upon reasonable request.

Declarations

Ethics approval This study was approved by the ethical committee of Ardabil University of Medical Sciences (IR.ARUMS.REC.1397.211).

Consent to participate Not applicable.

Consent for publication Not applicable.

Competing interests The authors declare no competing interests.

References

Abdolmalekia Z, Araba HA, Amanpourb S, Muhammadnejad S (2016) Anti-angiogenic effects of ethanolic extract of *Artemisia sieberi* compared to its active substance, artemisinin. Rev Bras Farmacogn 26:326–333

Adeola HA, Bano A, Vats R, Vashishtha A, Verma D, Kaushik D, Mittal V, Rahman MH, Najda A, Albadrani GM, Sayed AA, Farouk SM, Hassanein EHM, Akhtar MF, Saleem A, Abdel-Daim MM, Bhardwaj R (2021) Bioactive compounds and their libraries: an insight into prospective phytotherapeutics approach for oral mucocutaneous cancers. Biomed Pharmacother 141:111809

Akwii RG, Sajib MS, Zahra FT, Mikelis CM (2019) Role of angiopoietin-2 in vascular physiology and pathophysiology. Cells 8:471

Antfolk D, Sjoqvist M, Cheng F, Isoniemi K, Duran CL, Rivero-Muller A, Antila C, Niemi R, Landor S, Bouten CVC, Bayless KJ, Eriksson JE, Sahlgren CM (2017) Selective regulation of Notch ligands during angiogenesis is mediated by vimentin. Proc Natl Acad Sci U S A 114:E4574–E4581

Avicenna BL (2014) The Canon of Medicine (al-Qānūn Fī'l-ṭibb)(the Law of Natural Healing). Systemic diseases, orthopedics and cosmetics. Great Books of the Islamic World

Baharara J, Amini E, Mousavi M (2015) The anti-proliferative and anti-angiogenic effect of the methanol extract from brittle star. Rep Biochem Mol Biol 3:68–75

Blanco R, Gerhardt H (2013) VEGF and Notch in tip and stalk cell selection. Cold Spring Harb Perspect Med 3:a006569

Bohlooli S, Bohlooli S, Aslanian R, Nouri F, Teimourzadeh A (2015) Aqueous extract of *Agrostemma githago* seed inhibits caspase-3 and induces cell-cycle arrest at G1 phase in AGS cell line. J Ethnopharmacol 175:295–300

Caporarello N, Lupo G, Olivieri M, Cristaldi M, Cambria MT, Salmeri M, Anfuso CD (2017) Classical VEGF, Notch and Ang signalling in cancer angiogenesis, alternative approaches and future directions (Review). Mol Med Rep 16:4393–4402

Chen W, Xia P, Wang H, Tu J, Liang X, Zhang X, Li L (2019) The endothelial tip-stalk cell selection and shuffling during angiogenesis. J Cell Commun Signal 13:291–301

Chiu LC, Ooi VE, Sun SS (2001) Induction of apoptosis by a ribosome-inactivating protein from *Agrostemma githago* is associated with down-regulation of anti-apoptotic bcl-2 protein expression. Int J Oncol 19:137–141

Clochard J, Jerz G, Schmieder P, Mitdank H, Troger M, Sama S, Weng A (2020) A new acetylated triterpene saponin from Agrostemma githago L. modulates gene delivery efficiently and shows a high cellular tolerance. Int J Pharm 589:119822

Dai ZJ, Lu WF, Gao J, Kang HF, Ma YG, Zhang SQ, Diao Y, Lin S, Wang XJ, Wu WY (2013) Anti-angiogenic effect of the total flavonoids in *Scutellariabarbata* D Don. BMC Complement Altern Med 13:150

Deryugina EI, Quigley JP (2015) Tumor angiogenesis: MMP-mediated induction of intravasation- and metastasis-sustaining neovasculature. Matrix Biol 44–46:94–112

Dong Y, Zhang T, Li J, Deng H, Song Y, Zhai D, Peng Y, Lu X, Liu M, Zhao Y, Yi Z (2014) Oridonin inhibits tumor growth and metastasis through anti-angiogenesis by blocking the Notch signaling. PLoS ONE 9:e113830

Fan TP, Yeh JC, Leung KW, Yue PY, Wong RN (2006) Angiogenesis: from plants to blood vessels. Trends Pharmacol Sci 27:297–309

Foster S, Duke JA, Society NA, Peterson RT, Federation NW, Institute RTP (1990) A field guide to medicinal plants: Eastern and Central North America. Houghton Mifflin

Foubert K, Breynaert A, Theunis M, Van Den Bossche R, De Meyer GR, Van Daele A, Faizal A, Goossens A, Geelen D, Conway EM, Vlietinck A, Pieters L, Apers S (2012) Evaluation of the anti-angiogenic activity of saponins from *Maesa lanceolata* by different assays. Nat Prod Commun 7:1149–1154

Funahashi Y, Shawber CJ, Sharma A, Kanamaru E, Choi YK, Kitajewski J (2011) Notch modulates VEGF action in endothelial cells by inducing Matrix Metalloprotease activity. Vasc Cell 3:2

Garcia A, Kandel JJ (2012) Notch: a key regulator of tumor angiogenesis and metastasis. Histol Histopathol 27:151–156

Hassan LE, Ahamed MB, Majid AS, Baharetha HM, Muslim NS, Nassar ZD, Majid AM (2014) Correlation of antiangiogenic, antioxidant and cytotoxic activities of some Sudanese medicinal plants

with phenolic and flavonoid contents. BMC Complement Altern Med 14:406
Hiratsuka S, Nakamura K, Iwai SH, Murakami M, Itoh T, Kijima H, Shipley JM, Senior RM, Shibuya M (2002) MMP9 induction by vascular endothelial growth factor receptor-1 is involved in lung-specific metastasis. Cancer Cell 2:289–300
Jakobsson L, Bentley K, Gerhardt H (2009) VEGFRs and Notch: a dynamic collaboration in vascular patterning. Biochem Soc Trans 37:1233–1236
Jantova S, Topolska D, Janoskova M, Panik M, Milata V (2016) Study of the cytotoxic/toxic potential of the novel anticancer selenodiazoloquinolone on fibroblast cells and 3D skin model. Interdiscip Toxicol 9:106–112
Kim YW, Byzova TV (2014) Oxidative stress in angiogenesis and vascular disease. Blood 123:625–631
Kofler NM, Shawber CJ, Kangsamaksin T, Reed HO, Galatioto J, Kitajewski J (2011) Notch signaling in developmental and tumor angiogenesis. Genes Cancer 2:1106–1116
Koon YL, Zhang S, Rahmat MB, Koh CG, Chiam KH (2018) Enhanced delta-Notch lateral inhibition model incorporating intracellular Notch heterogeneity and tension-dependent rate of delta-Notch binding that reproduces sprouting angiogenesis patterns. Sci Rep 8:9519
Liang N, Li Y, Chung HY (2017) Two natural eudesmane-type sesquiterpenes from Laggera alata inhibit angiogenesis and suppress breast cancer cell migration through VEGF- and angiopoietin 2-mediated signaling pathways. Int J Oncol 51:213–222
Liu CT, Bi KW, Huang CC, Wu HT, Ho HY, JH SP, Huang ST, (2017) Davallia bilabiata exhibits anti-angiogenic effect with modified MMP-2/TIMP-2 secretion and inhibited VEGF ligand/receptors expression in vascular endothelial cells. J Ethnopharmacol 196:213–224
Liu Z, Fan F, Wang A, Zheng S, Lu Y (2014) Dll4-Notch signaling in regulation of tumor angiogenesis. J Cancer Res Clin Oncol 140:525–536
Loutrari H, Hatziapostolou M, Skouridou V, Papadimitriou E, Roussos C, Kolisis FN, Papapetropoulos A (2004) Perillyl alcohol is an angiogenesis inhibitor. J Pharmacol Exp Ther 311:568–575
Lu K, Bhat M, Basu S (2016) Plants and their active compounds: natural molecules to target angiogenesis. Angiogenesis 19:287–295
Lugano R, Ramachandran M, Dimberg A (2020) Tumor angiogenesis: causes, consequences, challenges and opportunities. Cell Mol Life Sci 77:1745–1770
M HR, Ghosh D, Banerjee R, Salimath BP (2017) Suppression of VEGF-induced angiogenesis and tumor growth by *Eugenia jambolana*, *Musa paradisiaca*, and *Coccinia indica* extracts. Pharm Biol 55(1):1489–1499. https://doi.org/10.1080/13880209.2017.1307422
Maes H, Olmeda D, Soengas MS, Agostinis P (2016) Vesicular trafficking mechanisms in endothelial cells as modulators of the tumor vasculature and targets of antiangiogenic therapies. FEBS J 283:25–38
Mahmoudinia S, Niapour A, Ghasemi Hamidabadi H, Mazani M (2019) 2,4-D causes oxidative stress induction and apoptosis in human dental pulp stem cells (hDPSCs). Environ Sci Pollut Res Int 26:26170–26183
Man S, Gao W, Zhang Y, Huang L, Liu C (2010) Chemical study and medical application of saponins as anti-cancer agents. Fitoterapia 81:703–714
Melzig MF, Hebestreit P, Gaidi G, Lacaille-Dubois MA (2005) Structure-activity-relationship of saponins to enhance toxic effects of agrostin. Planta Med 71:1088–1090
Min JK, Han KY, Kim EC, Kim YM, Lee SW, Kim OH, Kim KW, Gho YS, Kwon YG (2004) Capsaicin inhibits in vitro and in vivo angiogenesis. Cancer Res 64:644–651
Mohammadi-Motlagh HR, Shokohinia Y, Mojarrab M, Rasouli H, Mostafaie A (2017) 2-Methylpyridine-1-ium-1-sulfonate from *Allium hirtifolium*: an anti-angiogenic compound which inhibits growth of MCF-7 and MDA-MB-231 cells through cell cycle arrest and apoptosis induction. Biomed Pharmacother 93:117–129
Nam SH, Lkhagvasuren K, Seo HW, Kim JK (2017) Antiangiogenic effects of ziyuglycoside II, a major active compound of *Sanguisorba officinalis* L. Phytother Res 31:1449–1456
Niapour A, Bohlooli S, Sharifi Pasandi M, Mohammadi-ghalehbin B (2018) In vitro anti leishmanial effect of *Agrostemma githago* extract on leishmania major promastigotes by cell count and MTT assay. J Mazandaran Univ Med Sci 28:13–23
Niapour A, Ghasemi Hamidabadi H, Niapour N, Mohammadi P, Sharifi Pasandi M, Malekzadeh V (2019) Pharmacological Notch pathway inhibition leads to cell cycle arrest and stimulates ascl1 and neurogenin2 genes expression in dental pulp stem cells-derived neurospheres. Biotechnol Lett 41:873–887
Niapour A, Seyedasli N (2022) Acquisition of paclitaxel resistance modulates the biological traits of gastric cancer AGS cells and facilitates epithelial to mesenchymal transition and angiogenesis. Naunyn Schmiedebergs Arch Pharmacol 395:515–533
Niapour N, Niapour A, Sheikhkanloui Milan H, Amani M, Salehi H, Najafzadeh N, Gholami MR (2015) All trans retinoic acid modulates peripheral nerve fibroblasts viability and apoptosis. Tissue Cell 47:61–65
Phng LK, Gerhardt H (2009) Angiogenesis: a team effort coordinated by Notch. Dev Cell 16:196–208
Podolak I, Galanty A, Sobolewska D (2010) Saponins as cytotoxic agents: a review. Phytochem Rev 9:425–474
Saadati H, Noroozzadeh S, Esmaeili H, Amirshahrokhi K, Shadman J, Niapour A (2021) The neuroprotective effect of mesna on cisplatin-induced neurotoxicity: behavioral, electrophysiological, and molecular studies. Neurotox Res 39:826–840
Schrot J, Weng A, Melzig MF (2015) Ribosome-inactivating and related proteins. Toxins (basel) 7:1556–1615
Senger DR, Davis GE (2011) Angiogenesis. Cold Spring Harb Perspect Biol 3:a005090
Sharifi Pasandi M, Hosseini Shirazi F, Gholami MR, Salehi H, Najafzadeh N, Mazani M, Ghasemi Hamidabadi H, Niapour A (2017) Epi/perineural and Schwann cells as well as perineural sheath integrity are affected following 2,4-D exposure. Neurotox Res 32:624–638
Thomas JL, Baker K, Han J, Calvo C, Nurmi H, Eichmann AC, Alitalo K (2013) Interactions between VEGFR and Notch signaling pathways in endothelial and neural cells. Cell Mol Life Sci 70:1779–1792
Thurston G, Daly C (2012) The complex role of angiopoietin-2 in the angiopoietin-tie signaling pathway. Cold Spring Harb Perspect Med 2:a006550
Tian F, Zhang X, Tong Y, Yi Y, Zhang S, Li L, Sun P, Lin L, Ding J (2005) PE, a new sulfated saponin from sea cucumber, exhibits anti-angiogenic and anti-tumor activities in vitro and in vivo. Cancer Biol Ther 4:874–882
Tiemeijer LA, Ristori T, Stassen O, Ahlberg JJ, de Bijl JJJ, Chen CS, Bentley K, Bouten CVC, Sahlgren CM (2022) Engineered patterns of Notch ligands Jag1 and Dll4 elicit differential spatial control of endothelial sprouting. iScience 25:104306
Ugarte-Berzal E, Redondo-Munoz J, Eroles P, Del Cerro MH, Garcia-Marco JA, Terol MJ, Garcia-Pardo A (2010) VEGF/VEGFR2 interaction down-regulates matrix metalloproteinase-9 via STAT1 activation and inhibits B chronic lymphocytic leukemia cell migration. Blood 115:846–849
Velasquez C, Mansouri S, Mora C, Nassiri F, Suppiah S, Martino J, Zadeh G, Fernandez-Luna JL (2019) Molecular and clinical insights into the invasive capacity of glioblastoma cells. J Oncol 2019:1740763

Vincken JP, Heng L, de Groot A, Gruppen H (2007) Saponins, classification and occurrence in the plant kingdom. Phytochemistry 68:275–297

Wei J, Zhang L, Ren L, Zhang J, Yu Y, Wang J, Duan J, Peng C, Sun Z, Zhou X (2017) Endosulfan inhibits proliferation through the Notch signaling pathway in human umbilical vein endothelial cells. Environ Pollut 221:26–36

Woltje K, Jabs M, Fischer A (2015) Serum induces transcription of Hey1 and Hey2 genes by Alk1 but not Notch signaling in endothelial cells. PLoS ONE 10:e0120547

Xing Y, Tu J, Zheng L, Guo L, Xi T (2015) Anti-angiogenic effect of tanshinone IIA involves inhibition of the VEGF/VEGFR2 pathway in vascular endothelial cells. Oncol Rep 33:163–170

Yang Y, Duan W, Liang Z, Yi W, Yan J, Wang N, Li Y, Chen W, Yu S, Jin Z, Yi D (2013) Curcumin attenuates endothelial cell oxidative stress injury through Notch signaling inhibition. Cell Signal 25:615–629